Thin Plate Spline Image Registration in the Presence of Localized Landmark Errors

by

Eric Ng

Undergraduate Honours Thesis
Faculty of Science (Applied and Industrial Mathematics)
University of Ontario Institute of Technology

Supervisor(s): Dr. Mehran Ebrahimi

Abstract

Thin Plate Spline Image Registration in the Presence of Localized Landmark Errors

Eric Ng

Undergraduate Honours Thesis

Faculty of Science (Applied and Industrial Mathematics)

University of Ontario Institute of Technology

2017

The method of thin plate spline had been extensively used in the application of landmark-based image registration, where landmarks are placed on images of interest to represent sets of data points required for interpolation. Since these landmarks are often manually selected, their placements are highly susceptible to errors. Thus these errors in landmark placements lead to errors in the interpolating function. In this thesis, the mathematical background of thin plate splines will be explored by revisiting previous work by Duchon. Then, errors will be added to landmarks to observe the change in behaviour of the thin plate spline interpolant with the goal of obtaining an upper bound for its error. Preliminary results will be presented near the end of the thesis.

Contents

Chapter 1

Introduction

The alignment of multiple images against a single image is a procedure known as image registration. Image registration has significant importance in medical imaging as it enables matching of an object in different scenarios. For instance, multiple images of the same patient are taken to observe any biological and/or physiological changes that may occur over time. However, each series of images will experience some level of deformation due to a number of uncontrollable parameters. For example, figure 1.1 contain two images of a computed tomography (CT) scan of a human knee taken in two different points in time, where the first image may be taken during the patient's first visit, and the second image is taken during a follow-up appointment. It is evident that the knee had undergone significant movement in the second image. Hence initial diagnosis obtained using the first image may not translate over to the second image properly. Image registration bridges this gap by establishing a correspondence between the before and after images. This allows information obtained from the first image to be transferred to other images with accuracy.

Image registration is invaluable in matching images that undergo natural movement such as breathing patterns and tissue deformation from posture. In lung and heart imaging, the deformation is natural simply due to the different phases of breathing and

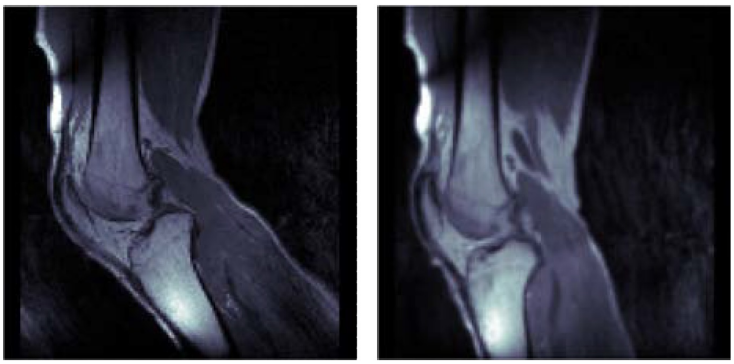

Figure 1.1: Computed tomography (CT) scan of a human knee. [6]

cardiac cycles respectively. By matching features and/or regions of interest in different images, not only does it allow information to be translated between the images, it also allows the prediction of surrounding deformation by imposing the appropriate constraints for the given scenario. This is especially crucial in the treatment of cancer, as images of tumours are captured over time. By registering these images against one another, this enables doctors to monitor, and sometimes even predict the growth of malignant tumours. In image-guided surgery, efficient and accurate registration methods are highly valued as diagnosis is determined using pre-operation images which do not reflect the patient's posture and/or position during a procedure. Registration that can be computed in realtime essentially enables pre-operation diagnosis to be brought into, and updated, in a surgical environment as opposed to relying strictly on the immediate discretion of the surgeon.

At minimum, image registration requires two images. In the simplest case, these two images are known as the reference image (source), and a template image (target). Ideally, we would like to find a transformation where the reference image under this transformation will match perfectly with the template image. In multi-frame registration, multiple reference images are chosen to be registered against a single template image as the name suggests. These images are typically taken from individual frames of a short video sequence. This method is usually chosen for situations where a single pair of

images do not provide sufficient information. Through having multiple input images, this allows additional information about the setting to be included at the cost of increased computational costs.

Methods for image registration are separated into two general categories: intensity based registration and feature based registration. As the names suggest, intensity based registration matches images using information obtained from the pixel intensities of the input images. This is typically treated by viewing the image as the discretization of a two dimensional signal, then applying the appropriate constraints (such as similarity measures, regularization, and boundary conditions) to recover the ideal transformation. As a result, the input images are considered as a whole which results in an unbiased global transformation. This is particularly useful for situations where registration is required across the majority of the images. On the other hand, feature based registration methods align images by placing sets of landmarks on both reference and template images. Each landmark in the reference image will have a corresponding landmark in the template image. This is used to physically identify features of interest on both images, and to associate a direct correspondence of one common region between the reference and the template. Unlike intensity based registration, feature based registration creates a bias at the locations where these landmarks are placed, as it explicitly dictates how the transformation must behave at these points. In turn, this preserves the geometrical structure during the registration procedure. As a result, this transformation is completely independent from pixel data. This enables registration between images taken from different modalities, such as computerized tomography (CT) and magnetic resonance (MR), which is a large advantage over intensity-based methods. An example shown in figure 1.2 presents a scenario where images of the brain were captured using different modalities (T1 versus T2 weighted MRI).

The primary focus of this thesis will be on landmark-based registration, in particular, using thin plate splines (TPS). The mathematical background of TPS and its properties

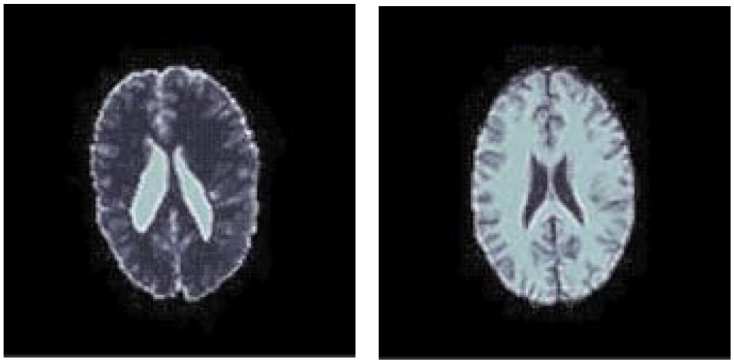

Figure 1.2: T1/T2 weighted MR scan of the brain. [6]

will be explored through revisiting the results from previous work by Duchon [3], Bookstein [1], and Wahba [7]. We will then continue by exploring how the TPS interpolant is affected if the given data suffers from errors.

Chapter 2

Thin Plate Spline (TPS)

2.1 Splines

Landmark-based registration is performed by finding a transformation that matches the one set of data points with the other set of data points under such transformation. If these data points match perfectly, then landmark-based registration is simply an interpolation problem in disguise. The problem then becomes finding a transformation that obeys these interpolating condition, while satisfying other constraints such as minimizing sudden deformations. The focus of this chapter will be on thin plate splines (TPS), one of the many landmark based registration methods that is widely used in medical imaging.

Splines are among one of the most popular methods of data interpolation. They are constructed as piecewise polynomials where continuity and differentiability up to a certain order is preserved at the points where the sub-polynomials meet. For example, a cubic spline is a piecewise cubic function, where continuity and differentiability up to second order is preserved at the ends of each sub-function. By preserving differentiability at the ends of each piece, it imposes a smoothing condition against the spline based on the highest order derivative that is preserved.

Unlike traditional splines, thin plate spline (TPS) is a spline interpolation method

where the smoothness of the spline is controlled by a gradient based regularization term. This regularization is designed to simulate the energy required to bend a thin sheet of metal. This is reflected in the choice of basis functions in the interpolant. This interpolant comprises of an affine part which controls the overall shape of the spline, and a non-linear part using radial basis functions to produce deformations. The radial basis functions are based on the fundamental solution of the biharmonic operator, a fourth order partial differential operator that is highly similar to the spatial component of the homogeneous Euler-Bernoulli beam equation.

2.2 Mathematical Background

In this section, the mathematical formulation of thin plate spline will be explored. To begin, let $\{r_j\}, \{t_j\}, j = 1, \ldots, n$ represent the two different sets of data points. We want to find a smooth function $f : \Omega \subset \mathbb{R}^d \to \mathbb{R}^d$ that satisfies the interpolation conditions

$$f(r_j) = t_j, \quad j = 1, \ldots, n. \tag{2.1}$$

As long as these conditions are met, it is immediately a minimizer of the functional

$$\mathcal{T}[f] = \sum_{j=1}^{n} \|f(r_j) - t_j\|_2^2 \tag{2.2}$$

where $\|\cdot\|_2$ is the Euclidean 2-norm. The smoothness of this interpolating function will vary depending on how spread out the data points are. Data points that are spread out will yield a smoother result as opposed to data points that are clustered together. This smoothness can also be controlled by adding a gradient based regularization term at the expense of losing the interpolating conditions. The combination of the interpolation conditions and regularization produces the objective functional

$$\mathcal{J}[f] = \sum_{j=1}^{n} \|f(r_j) - t_j\|_2^2 + \lambda \int_{\Omega} |\nabla^m f|^2 dx \tag{2.3}$$

where Ω is the domain of the image. The function f that minimizes 2.3 is known as the polyharmonic spline. Thin plate spline (TPS) is one specific case of the polyharmonic spline by choosing $m = 2$. The smoothness of the result is controlled by the parameter $\lambda \geq 0$. In particular, the thin plate spline interpolant minimizes the following specific objective functional

$$\mathcal{J}[f] = \sum_{j=1}^{n} \|r_j - f(t_j)\|_2^2 + \lambda \int_{\Omega} \Big[\Big(\frac{\partial^2 f}{\partial x_1^2} \Big)^2 + 2 \Big(\frac{\partial^2 f}{\partial x_1 \partial x_2} \Big)^2 + \Big(\frac{\partial^2 f}{\partial x_2^2} \Big)^2 \Big] dx \tag{2.4}$$

This spline method was originally designed by Duchon [3] to obtain a closed form solution for thin plate spline. Wahba [7] later proved the existence of a unique minimizer for the above variational problem. This unique solution has a representation as a linear combination of a affine and a non-affine part of the form

$$f(x) = a_0 + a_1 x_1 + a_2 x_2 + \sum_{j=1}^{n} c_j \phi(\|x - r_j\|_2) \tag{2.5}$$

where $x = (x_1, x_2) \in \mathbb{R}^2$ and $\phi(r) = \frac{1}{8\pi} r^2 \ln r$ is the fundamental solution of the biharmonic harmonic operator, i.e. $\Delta^2 \phi = \delta_{(0,0)}$. In many literature, $\phi(r)$ is often seen as $\phi(r) = r^2 \ln r$ as the pre-factor is typically absorbed into the coefficient. $\phi(r)$ are frequently called radial basis functions, as it serves as a family of nonlinear basis functions in the interpolant that are radially symmetric. The non-affine part of the solution is responsible for the local deformations of the spline caused by the data points. At the infinities, these non-affine components vanishes to 0 which causes the spline to be characterized by the affine part of the solution at locations far away from the data points. Note that by choosing f to be in this form, there is now a unique solution to 2.2 as it was ill-posed if f was chosen from the space of all continuous functions.

In the context of image registration, the sets of data points $\{r_j\}$ and $\{t_j\}$ are often referred to as landmarks on the reference and template images respectively. For simplicity, we will focus on the 2-dimensional case ($d = 2$) but it can extended to higher dimensional images with relative ease. Since the radial basis functions of the interpolant are centred

around the reference landmarks, these landmarks are sometimes referred to as centres. It shall be noted that throughout this thesis, any *superscripts* that appear in coefficients and landmarks will denote the corresponding spatial dimension unless otherwise indicated. The two coordinate directions will simply be x_1 and x_2.

2.3 Coefficients of TPS Interpolant

Recall from the previous section that TPS is a linear combination of an affine and non-affine part as shown in equation 2.5. The solution spline is fully determined by the coefficients obtained using the given data points. As an interpolation problem, each reference and template landmark must satisfy the condition

$$t_j = f(r_j) = a_0 + a_1 r_j^1 + a_2 r_j^2 + \sum_{i=1}^{n} c_j \phi(\|r_j - r_i\|_2). \tag{2.6}$$

The collection of this condition against every landmark results in the linear system

$$\begin{pmatrix} \phi(\|r_1 - r_1\|_2) & \phi(\|r_1 - r_2\|_2) & \dots & \phi(\|r_1 - r_n\|_2) & 1 & r_1^1 & r_1^2 \\ \phi(\|r_2 - r_1\|_2) & \phi(\|r_2 - r_2\|_2) & \dots & \phi(\|r_2 - r_n\|_2) & 1 & r_2^1 & r_2^2 \\ \vdots & \vdots & \ddots & \vdots & \vdots & \vdots & \vdots \\ \phi(\|r_n - r_1\|_2) & \phi(\|r_n - r_2\|_2) & \dots & \phi(\|r_n - r_n\|_2) & 1 & r_n^1 & r_n^2 \end{pmatrix} \begin{pmatrix} c_1 \\ \vdots \\ c_n \\ a_0 \\ a_1 \\ a_2 \end{pmatrix} = \begin{pmatrix} t_1 \\ t_2 \\ \vdots \\ t_n \end{pmatrix}. \tag{2.7}$$

For compactness, we can the define the matrices and vectors

$$A = \begin{pmatrix} \phi(\|r_1 - r_1\|_2) & \phi(\|r_1 - r_2\|_2) & \dots & \phi(\|r_1 - r_n\|_2) \\ \phi(\|r_2 - r_1\|_2) & \phi(\|r_2 - r_2\|_2) & \dots & \phi(\|r_2 - r_n\|_2) \\ \vdots & \vdots & \ddots & \vdots \\ \phi(\|r_n - r_1\|_2) & \phi(\|r_n - r_2\|_2) & \dots & \phi(\|r_n - r_n\|_2) \end{pmatrix}, \tag{2.8}$$

$$B = \begin{pmatrix} 1 & 1 & \dots & 1 \\ r_1^1 & r_2^1 & \dots & r_n^1 \\ r_1^2 & r_2^2 & \dots & r_n^2 \end{pmatrix}^T, \tag{2.9}$$

$$\mathbf{c} = (c_1, c_2, \dots, c_n)^T, \tag{2.10}$$

$$\mathbf{a} = (a_0, a_1, a_2)^T, \tag{2.11}$$

$$\mathbf{t} = (t_1, t_2, \dots, t_n)^T \tag{2.12}$$

which reduces the expansion to

$$(A \mid B)(\mathbf{c}, \mathbf{a})^T = \mathbf{t}. \tag{2.13}$$

This gives us n equations for $n+3$ unknowns. A non-singular system can be constructed by adding the constraints

$$\sum_{j=1}^{n} c_j = 0, \tag{2.14}$$

$$\sum_{j=1}^{n} c_j r_j^1 = 0, \tag{2.15}$$

$$\sum_{j=1}^{n} c_j r_j^2 = 0. \tag{2.16}$$

These constraints are added as orthogonality conditions that ensure the deformation created by the non-linear radial basis functions are in the direction orthogonal to the affine part of the spline. In addition, these constraints also imposes a condition where the higher order derivatives of the $\phi(r)$ vanishes to zero as $r \to \infty$, which gives the property that the spline asymptotically approaches the affine part of the solution. Its mathematical details will be explored on in the later part of this section. In summary, The thin plate spline coefficients are then determined by solving the block linear system

$$\begin{pmatrix} A & B \\ B^T & \mathbf{0} \end{pmatrix} \begin{pmatrix} \mathbf{c} \\ \mathbf{a} \end{pmatrix} = \begin{pmatrix} \mathbf{t} \\ \mathbf{0} \end{pmatrix}. \tag{2.17}$$

Note that this matrix has no dependency on the regularization parameter λ which corresponds to a direct interpolation against the radial basis functions. We want to determine a generalized system that is dependent on λ which also agrees with the matrix above when $\lambda = 0$. To do this, we first rewrite the interpolation condition in the objective function from equation 2.3 in terms of delta functions. This gives us

$$\sum_{j=1}^{n} \|f(r_j) - t_j\|_2^2 = \int_\Omega \sum_{j=1}^{n} \|f(x) - t_j\|_2^2 \delta(x - r_j) dx. \tag{2.18}$$

Applying this to equation 2.4 rewrites the TPS objective functional as

$$\mathcal{J}[f] = \int_\Omega \left(\sum_{j=1}^{n} \|f(x) - t_j\|_2^2 \delta(x - r_j) + \lambda \left[\left(\frac{\partial^2 f}{\partial x_1^2} \right) + 2 \left(\frac{\partial^2 f}{\partial x_1 x_2} \right)^2 + \left(\frac{\partial^2 f}{\partial x_2^2} \right)^2 \right] \right) dx. \tag{2.19}$$

Let $F(x, f, \partial^{\alpha_1} f, \partial^{\alpha_2} f, \partial^{\alpha_3} f)$ be the integrand above, where $\alpha = (\alpha_1, \alpha_2, \alpha_3)$ is a multi-index across all second order partial derivatives of f. Then the function f that minimizes the above variational problem must satisfy the corresponding Euler-Lagrange equation

$$\frac{\partial F}{\partial f} + \frac{\partial^2}{\partial x_1^2} \left(\frac{\partial F}{\partial (\partial^{\alpha_1} f)} \right) + \frac{\partial^2}{\partial x_1 \partial x_2} \left(\frac{\partial F}{\partial (\partial^{\alpha_2} f)} \right) + \frac{\partial^2}{\partial x_2^2} \left(\frac{\partial F}{\partial (\partial^{\alpha_3} f)} \right) = 0, \tag{2.20}$$

where

$$\partial^{\alpha_1} f = \frac{\partial^2 f}{\partial x_1^2}, \tag{2.21}$$

$$\partial^{\alpha_2} f = \frac{\partial^2 f}{\partial x_1 \partial x_2}, \tag{2.22}$$

$$\partial^{\alpha_3} f = \frac{\partial^2 f}{\partial x_2^2}. \tag{2.23}$$

Computing each derivative explicitly, we have

$$\frac{\partial F}{\partial f} = 2 \sum_{j=1}^{n} \|f(x) - t_j\|_2 \delta(x - r_j), \tag{2.24}$$

$$\frac{\partial^2}{\partial x_1^2} \left(\frac{\partial F}{\partial (\partial^{\alpha_1} f)} \right) = 2\lambda \frac{\partial^4 f}{\partial x_1^4}, \tag{2.25}$$

$$\frac{\partial^2}{\partial x_1 \partial x_2} \left(\frac{\partial F}{\partial (\partial^{\alpha_2} f)} \right) = 4\lambda \frac{\partial^4 f}{\partial x_1^2 \partial x_2^2}, \tag{2.26}$$

$$\frac{\partial^2}{\partial x_2^2} \left(\frac{\partial F}{\partial (\partial^{\alpha_3} f)} \right) = 2\lambda \frac{\partial^4 f}{\partial x_2^4}. \tag{2.27}$$

Then the corresponding Euler-Lagrange equation is

$$\sum_{j=1}^{n} \|f(x) - t_j\|_2 \delta(x - r_j) + \lambda \left[\frac{\partial^4 f}{\partial x_1^4} + 2\frac{\partial^4 f}{\partial x_1^2 \partial x_2^2} + \frac{\partial^4 f}{\partial x_2^4} \right] = 0, \tag{2.28}$$

or more compactly

$$\sum_{j=1}^{n} \|f(x) - t_j\|_2 \delta(x - r_j) + \lambda \Delta^2 f = 0. \tag{2.29}$$

Now consider any test function $\psi(x)$ such that $\text{supp}(\psi) = \Omega$, then $f(x)$ is consider a weak solution if the following holds

$$\int_\Omega \left(\sum_{j=1}^{n} \|f(x) - t_j\|_2 \delta(x - r_j)\psi(x) + \lambda(\Delta^2 f)\psi(x) \right) dx = 0. \tag{2.30}$$

To extract a delta function from the second term of the integral, we applying the Δ^2 operator against f in equation 2.5. Since Δ^2 is a fourth order differential operator, we can immediately conclude that the affine part will disappear. Furthermore, the non-affine part contains a linear combination of the fundamental solution of the operator itself. The reduces the result to a linear combination of delta functions. Hence

$$\begin{aligned} \Delta^2 f &= \Delta^2 \sum_{j=1}^{n} c_j \phi(\|x - r_j\|_2) \\ &= 8\pi \sum_{j=1}^{n} c_j \delta(x - r_j). \end{aligned} \tag{2.31}$$

Applying this to 2.30 will give us

$$\int_\Omega \left(\sum_{j=1}^{n} \|f(x) - t_j\|_2 \delta(x - r_j)\psi(x) + 8\pi\lambda \sum_{j=1}^{n} c_j \delta(x - r_j)\psi(x) \right) dx = 0. \tag{2.32}$$

The delta functions are then removed through integration

$$\sum_{j=1}^{n} \left(\|f(x) - t_j\|_2 + 8\pi\lambda c_j \right) \psi(r_j) = 0. \tag{2.33}$$

In order for 2.33 to hold for all test functions ψ, then the term in the parenthesis must be 0 which gives the condition

$$\|f(x) - t_j\|_2 + 8\pi\lambda c_j = 0 \tag{2.34}$$

for all $j = 1, \ldots, n$. Since $\lambda > 0$ is an arbitrary constant, 8π can be absorbed into the regularization parameter. By invoking the original interpolation condition to the equation above, this allows us to include the regularization parameter into the interpolation matrix by replacing A with $A + \lambda I$, where I is the $n \times n$ identity matrix. This generalizes the solution to any thin plate spline problem as the solution to the linear system

$$\begin{pmatrix} A + \lambda I & B \\ B^T & \mathbf{0} \end{pmatrix} \begin{pmatrix} \mathbf{c} \\ \mathbf{a} \end{pmatrix} = \begin{pmatrix} \mathbf{t} \\ \mathbf{0} \end{pmatrix}. \tag{2.35}$$

We now proceed to show that the interpolating matrix is invertible. We begin by the introducing the definition of complete monotonicity.

Definition 2.3.1 (Completely Monotone)**.** *Let $\varphi \in C[0, \infty) \cap C^\infty(0, \infty)$, where $\varphi : [0, \infty) \to \mathbb{R}$. φ is called* completely monotone *on $[0, \infty)$ if it satisfies*

$$(-1)^\ell \varphi^{(\ell)}(r) \geq 0, \quad r > 0, \quad \ell = 0, 1, 2, \ldots$$

In addition, the following theorems are necessary to deduce that the interpolating matrix is non-singular

Theorem 2.3.1 (Hausdorff-Bernstein-Widder)**.** *Let $\Psi \in C[0, \infty)$. Then Ψ is completely monotone if and only if it is the Laplace transform of a Borel probability measure on*

$$[0, \infty)$$

.

A variation of this theorem states that Ψ is completely monotone if and only if it is the Laplace transform of an admissible function $w(x)$.

Theorem 2.3.2. *Let $\phi = C[0, \infty)$ and $\psi := \phi(\sqrt{\cdot})$. Suppose that for some non-negative integer m so that $\psi^{(m+1)}$ is strictly monotone, then the matrix $(-1)^{(m+1)}A$ is positive definite on the subspace*

$$S_m(X) := \{\mathbf{c} \in \mathbb{R}^n : \sum_{j=1}^{n} c_j p(x_j) = 0\}$$

where $p(x)$ is a polynomial of degree at most m, and A is the matrix with elements $a_{ij} = \psi(\|x_i - x_j\|)$.

Detailed proofs of these theorems can be found in books by Cheney and Light [2]. For thin plate splines, we consider the radial basis function $\phi(r)$ used for the interpolant. We can define $\psi(r) = \phi(\sqrt{r}) = r\ln(r)$. Notice that $\psi^{(m+1)}$ is monotone for every $m \geq 1$, with $\psi^{(2)}(m+1) = 1/2r$ with the corresponding admissible function $w(x) = 1/2$ by the Hausdorff-Bernstein-Widder theorem. The second theorem indicates that the matrix A that was originally constructed must be positive definite on the subspace $S_1(X)$: the subspace of linear polynomials. This dictates the conditions imposed by the bottom block of the interpolating linear system.

Theorem 2.3.3. *Suppose A is positive definite on $\ker(B^T)$ and the columns of B are linearly independent, then the block matrix*

$$\begin{pmatrix} A & B \\ B^T & \mathbf{0} \end{pmatrix}$$

is non-singular.

Proof. We show that the block matrix is invertible by showing that it has a trivial nullspace. Suppose that

$$\begin{pmatrix} A & B \\ B^T & \mathbf{0} \end{pmatrix} \begin{pmatrix} \mathbf{c} \\ \mathbf{a} \end{pmatrix} = \mathbf{0},$$

this gives us the coupled equations $A\mathbf{c} + B\mathbf{a} = 0$ and $B^T\mathbf{c} = 0$. The second equation says that $\mathbf{c} \in \ker(B^T)$. We then multiply the first equation by $\mathbf{c}^T$

$$\mathbf{c}^T A\mathbf{c} + \mathbf{c}^T B\mathbf{a} = 0.$$

However,

$$\mathbf{c}^T B = 0$$

since this is simply the transpose of the bottom block equation. Therefore

$$\mathbf{c}^T A\mathbf{c} + \mathbf{c}^T B\mathbf{a} = \mathbf{c}^T A\mathbf{c} = 0.$$

However, $\mathbf{c}$ must be the zero vector since A is positive definite against $\ker(B^T) \ni \mathbf{c}$. Therefore, the first equation from the top matrix block becomes $B\mathbf{a} = \mathbf{0}$. Since the columns of B are linearly independent columns, then B must be full rank. This implies that $B\mathbf{a} = \mathbf{0}$ holds if and only if $\mathbf{a} = \mathbf{0}$. Hence the only solution to the homogeneous system is $[\mathbf{c}, \mathbf{a}]^T = \mathbf{0}$ which concludes that the block matrix must be non-singular. □

This indicates that the interpolation problem becomes well-posed as long as B is full rank. Recall that B is constructed using the coordinates of the reference landmarks as its elements, then this requirement is satisfied by ensuring that the chosen landmarks are not co-linear. Similar to many other problems involving large linear systems, the inverse of the matrix is never computed explicitly. Instead, the coefficient vectors are recovered by more efficient numerical methods such as LU decomposition, or Cholesky decomposition. To observe the behaviour and shape of the thin plate spline, a toybox model is constructed using the following data points:

$$\{r_j\} = \{(-1, 1), (1, -1), (1, 1), (-1, 1)\}$$
$$\{t_j\} = \{(-0.63, -1.32), (1.41, -0.94), (0.72, 1.18), (-1.21, 0.82)\}$$

Figure 2.1 shows the TPS interpolant obtained using the data points listed above for parameter values $\lambda = 0, 5, 10$. It can be seen that the deformations of the spline occur near the centres of the radial basis functions, then approaches the linear plane as the distance to these centres become large. As the regularization parameter λ increases, the local deformations caused by the non-linear terms of the spline shrinks. In the limiting case as $\lambda \to \infty$, the spline becomes a flat plane, which corresponds to the least square fit of the data points to a plane.

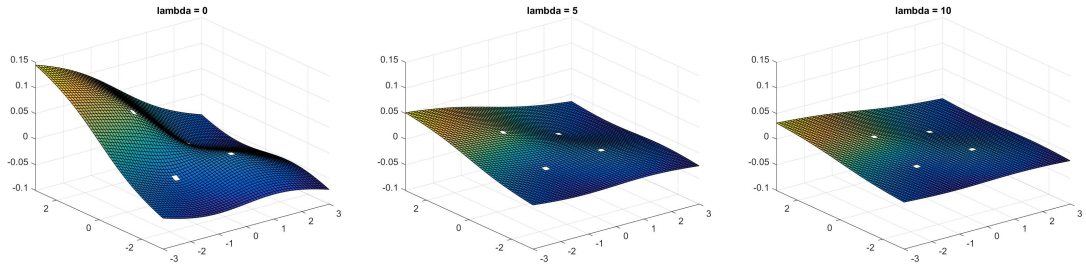

Figure 2.1: Thin Plate Spline with various λ values.

2.4 Application of TPS in Image Registration

In image registration, thin plate spline is used to model the displacement of landmarks. In particular, it interpolates the coordinate displacement of each pixel of the image as it is crucial that the geometric structure of the image is preserved. Therefore, for each 2-dimensional image registration problem, there will be two different thin plate spline interpolants, where the first spline models the coordinate changes in the x_1 direction, and the second spline models the coordinate changes in the x_2 direction. In the previous section, it was shown that obtaining the coefficients of a TPS problem reduces to solving a single matrix-vector system. Since this matrix contain no dependency on the template landmarks, this system can be easily extended to obtain all the coefficients required for each spline in a single step. This is done by modifying the existing matrix-vector system to a matrix-matrix system through augmenting the solution vector into a $n \times 2$ solution matrix. More explicitly, the linear system now becomes

$$\begin{pmatrix} A + \lambda I & B \\ B^T & \mathbf{0} \end{pmatrix} \begin{pmatrix} \mathbf{c}^1 & \mathbf{c}^2 \\ \mathbf{a}^1 & \mathbf{a}^2 \end{pmatrix} = \begin{pmatrix} \mathbf{t}^1 & \mathbf{t}^2 \\ \mathbf{0} & \mathbf{0} \end{pmatrix} \tag{2.36}$$

where $[\mathbf{c}^i, \mathbf{a}^i]^T$ and $\mathbf{t}^i$ are the vector of the thin plate spline coefficients and template landmark locations in the i'th coordinate direction. As a result, the thin plate spline

interpolants of a 2-dimensional registration problem can be characterized by

$$f^1(x) = a_0^1 + a_1^1 x_1 + a_2^1 x_2 + \sum_{j=1}^{n} c_j^1 \phi(\|x - r_j\|_2), \tag{2.37}$$

$$f^2(x) = a_0^1 + a_1^1 x_1 + a_2^1 x_2 + \sum_{j=1}^{n} c_j^2 \phi(\|x - r_j\|_2). \tag{2.38}$$

Figure 2.2 is a practical application of landmark registration using thin plate spline

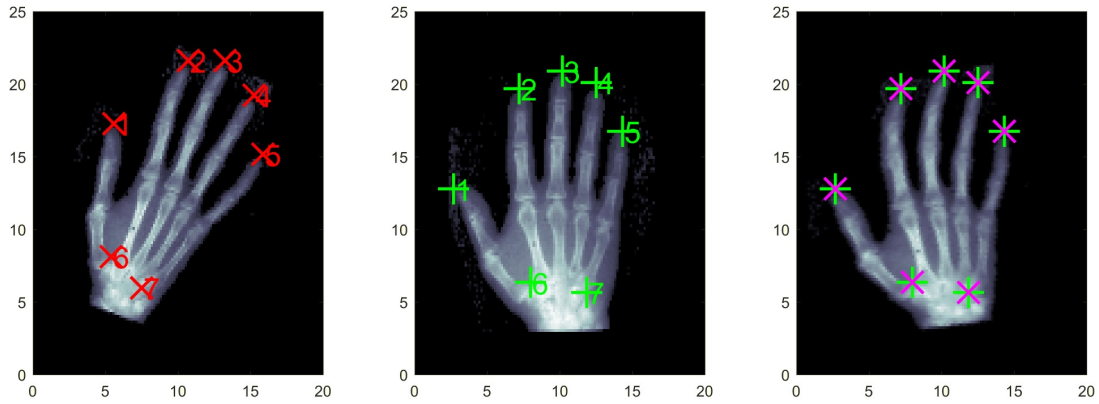

Figure 2.2: TPS registration: X-Ray of a hand, $\lambda = 0$. [6]

where the left, centre, and right images are the reference image, template image, and the transformed reference image respectively. The sets of landmarks $\{r_j\}$ and $\{t_j\}$ are shown using red and green markers, with the adjacent number identifying the correspondence between these landmarks. In the right image, registration takes place where the reference image is transformed to line up with the template image under the constraints imposed through TPS. Note that in the transformed image, the corresponding landmarks line up perfectly. This indicates that $f(r_j) = t_j$ for all $j = 1, \ldots, n$. Thus this corresponds to TPS registration using $\lambda = 0$.

Figure 2.3 is the same registration problem with $\lambda = 1000$. It can be seen in this case that the landmarks no longer line up perfectly. This indicates that the original interpolating conditions are lost as the numerical value of λ increases. However, despite the misalignment of the landmarks, there is a visual improvement in the registration

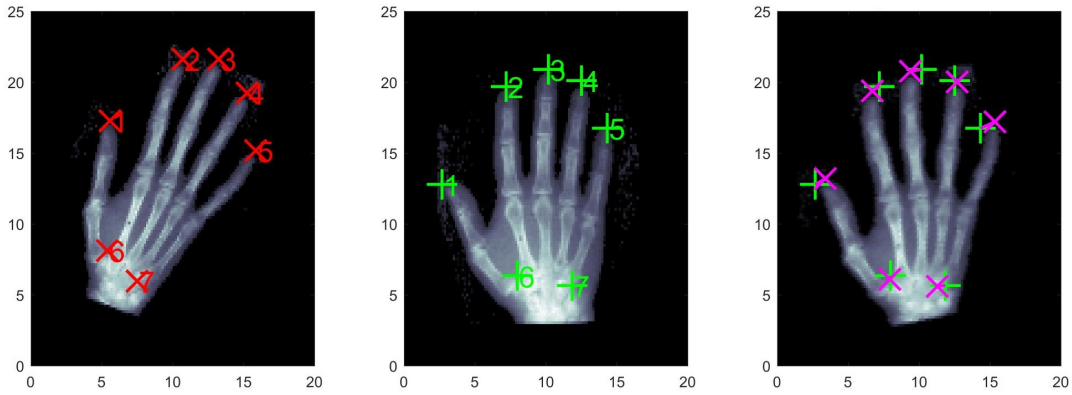

Figure 2.3: TPS registration: X-Ray of a hand, $\lambda = 1000$. [6]

result. This is due to the skeletal structure of the hand, as the bones should undergo a rigid transformation as opposed to a transformation simulating the bending of a thin metal plate. By raising the value of λ, the affine part of the registration scheme overtakes the non-linear deformation which experiences less bending. This in turn preserves the rigidness of the bones themselves.

Note that these examples are included in the textbook of Modersitzki, Flexible Algorithms for Image Registration (FAIR) [6], and requires a licensed version of MATLAB to replicate the examples.

Chapter 3

Errors in Landmarks

3.1 Motivation

As indicated before, thin plate splines are highly useful in landmark-based medical image registration. These landmarks are placed either manually as physical landmarks, or automatically by a computer through a feature-identifying algorithm. In both cases, errors of landmark placements are naturally very likely to occur. This may be caused by a number of reasons, such as misplacement of physical landmarks (human error), error in detection of landmarks (machine error), or sometimes even natural errors such as the breathing cycle of the patient. Therefore, it is beneficial to determine a confidence in the registration result based on the confidence in the given landmarks.

To investigate how errors affect the interpolant, errors were randomly generated from a uniform distribution and were applied each template landmark in the hand example from the previous chapter. These errors are bounded above by 2 in a 20×25 domain.

Figure 3.1 shows a comparison between TPS registration results using the original landmarks, and landmarks that were exposed to errors. It can be seen in the second image that the fingers in the second image are bending in unnatural ways due to the errors added onto the landmarks. This gives an incentive on analyzing the change in

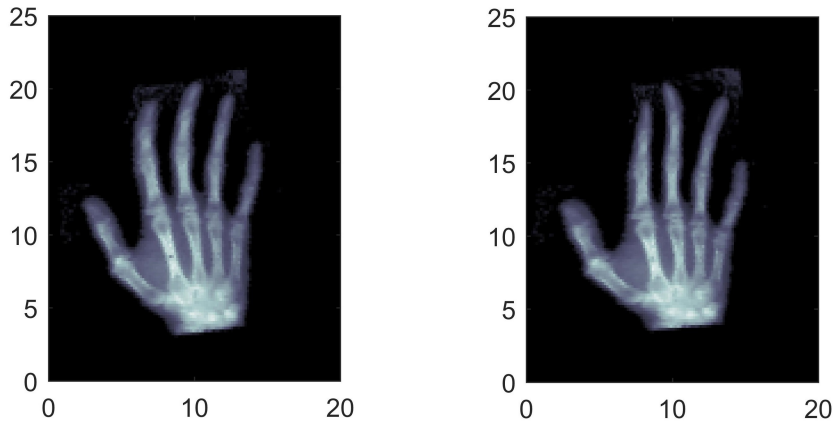

Figure 3.1: Comparison of original (left) and error prone (right) TPS interpolant.

the interpolant due to landmark errors as it may lead to potential misdiagnosis. In this chapter, we will explore how the interpolants are affected by imposing small random errors to individual landmarks, where the magnitude of these errors will be bounded by some small fixed value. We will aim to provide an upper bound to absolute difference between the two TPS interpolants.

3.2 Error Analysis of TPS

In Chapter 2, we visited the mathematical background of TPS, where the coefficients of the interpolant are determined by solving the linear system

$$\begin{pmatrix} A + \lambda I & B \\ B^T & \mathbf{0} \end{pmatrix} \begin{pmatrix} \mathbf{c} \\ \mathbf{a} \end{pmatrix} = \begin{pmatrix} \mathbf{t} \\ \mathbf{0_3} \end{pmatrix} \tag{3.1}$$

where the first matrix is represented by L. This matrix, by construction, is only dependent on the reference landmarks $\{r_j\}$, and independent from the template landmarks $\{t_j\}$. In addition, the closed form solution of the TPS interpolant is also independent of the template landmarks, by using reference landmarks as the centres of the radial basis

functions. By adding errors to the template landmarks only, this preserves the structure of the matrix L and the basis functions of the interpolant. The changes in the interpolant will then be fully characterized by how the TPS coefficients change as errors are introduced to the template landmarks. Suppose that for every template landmark $\{t_j\}$, an error term ϵ_j^i is added in the i'th spatial dimension, with $|\epsilon_j^i| < \epsilon \; \forall j = 1, \ldots, n, \; \epsilon > 0$, i.e. the magnitude of the errors are bounded by a fixed positive number. Since the reference landmarks were unchanged, then this new TPS will be in the form

$$g^i(x) = \tilde{a}_0^i + \tilde{a}_1^i x_1 + \tilde{a}_2^i x_2 + \sum_{j=1}^{n} \tilde{c}_j^i \phi(\|x - r_j\|_2). \tag{3.2}$$

This allows us to define the error function

$$\begin{aligned} E^i(x) &= |g^i(x) - f^i(x)| \\ &= \left| (\tilde{a}_0^i - a_0^i) + (\tilde{a}_1^i - a_1^i)x_1 + (\tilde{a}_2^i - a_2^i)x_2 + \sum_{j=1}^{n} (\tilde{c}_j^i - c_j^i)\phi(\|x - r_j\|_2) \right| \end{aligned} \tag{3.3}$$

which is the error function that we wish to find the upper bound for. Note that this error function is also in the form of a TPS interpolant. Therefore, these coefficients can be solved using the regular thin plate spline method. Let $\tilde{\mathbf{c}}^i, \tilde{\mathbf{a}}^i$ represent the coefficients associated with the TPS interpolant subject to errors, then we can solve for the coefficient vectors $\tilde{\mathbf{a}}^i$ and $\tilde{\mathbf{c}}^i$ through the following linear system.

$$L \begin{pmatrix} \tilde{\mathbf{c}}^i \\ \tilde{\mathbf{a}}^i \end{pmatrix} = \begin{pmatrix} \mathbf{t}^i + \varepsilon^i \\ \mathbf{0} \end{pmatrix} \tag{3.4}$$

where $\varepsilon^i = (\epsilon_1^i, \ldots, \epsilon_n^i)^T$ is a vector of errors. Then

$$\begin{aligned} \begin{pmatrix} \tilde{\mathbf{c}}^i \\ \tilde{\mathbf{a}}^i \end{pmatrix} &= L^{-1} \begin{pmatrix} \mathbf{t}^i + \varepsilon^i \\ \mathbf{0} \end{pmatrix} \\ &= L^{-1} \begin{pmatrix} \mathbf{t}^i \\ \mathbf{0} \end{pmatrix} + L^{-1} \begin{pmatrix} \varepsilon^i \\ \mathbf{0} \end{pmatrix} \\ &= \begin{pmatrix} \mathbf{c}^i \\ \mathbf{a}^i \end{pmatrix} + L^{-1} \begin{pmatrix} \varepsilon^i \\ \mathbf{0}^i \end{pmatrix} \end{aligned}$$

From here we can see that

$$\begin{pmatrix} \tilde{\mathbf{c}}^{\mathbf{i}} - \mathbf{c}^{\mathbf{i}} \\ \tilde{\mathbf{a}}^{\mathbf{i}} - \mathbf{a}^{\mathbf{i}} \end{pmatrix} = L^{-1} \begin{pmatrix} \varepsilon^i \\ \mathbf{0} \end{pmatrix}. \tag{3.5}$$

Using a norm-based approach, we deduce the following:

$$\begin{aligned} E^i(x) &= \left| (\tilde{a}_0^i - a_0^i) + (\tilde{a}_1^i - a_1^i)x_1 + (\tilde{a}_2^i - a_2^i)x_2 + \sum_{j=1}^{n} (\tilde{c}_j^i - c_j^i)\phi(\|x - r_j\|_2) \right| \\ &\leq \left\| \begin{pmatrix} \tilde{\mathbf{a}}^i - \mathbf{a}^i \\ \tilde{\mathbf{c}}^i - \mathbf{c}^i \end{pmatrix} \right\|_2 \left\| \begin{pmatrix} \phi(\|x - r_j\|_2) \\ \mathbf{x}^i \end{pmatrix} \right\|_2 \quad \text{(Cauchy-Schwarz Inequality)} \\ &= \left\| L^{-1} \begin{pmatrix} \varepsilon^i \\ \mathbf{0} \end{pmatrix} \right\|_2 \left\| \begin{pmatrix} \phi(\|x - r_j\|_2) \\ \mathbf{x}^i \end{pmatrix} \right\|_2 \\ &\leq \|L^{-1}\|_2 \|\varepsilon^i\|_2 \left\| \begin{pmatrix} \phi(\|x - r_j\|_2) \\ \mathbf{x}^i \end{pmatrix} \right\|_2 \end{aligned} \tag{3.6}$$

We now evaluate each individual norms. For any square matrix A, since $\|A\|_2^2 = \rho(A^T A)$, where $\rho(A)$ is the spectral radius of A, i.e. its largest eigenvalue, then

$$\begin{aligned} \|L^{-1}\|_2 &= \sqrt{\rho((L^{-1})^T L^{-1})} \\ &= \sqrt{\rho((L^T)^{-1} L^{-1})} \\ &= \sqrt{\rho((LL^T)^{-1})} \\ &= \sqrt{\mu_{max}(L^T L)^{-1}} \\ &= \frac{1}{\sqrt{\mu_{min}(L^T L)}} \\ &= \frac{1}{\sigma_{min}(L)} \end{aligned} \tag{3.7}$$

where μ and σ denotes the eigenvalues and singular values of L. For the second norm, we have

$$\begin{aligned} \|\varepsilon^i\|_2^2 &= \sum_{j=1}^{n} |\epsilon_j^i|^2 \\ &\leq n\epsilon^2. \end{aligned} \tag{3.8}$$

Therefore $\|\varepsilon^i\|_2 \leq \sqrt{n}\epsilon$. For the third norm, note that the norm diverges to infinity as x approaches infinity. Hence it is impossible to obtain an upper bound unless the domain is restricted to a bounded subset of $\mathbb{R}^2$. By applying equations 3.7 and 3.8 to equation 3.6, we obtain an upper bound for $E^i(x)$ as

$$E^i(x) \leq \frac{\sqrt{n}\epsilon}{\sigma_{min}(L)} \left\| \begin{pmatrix} \phi(\|x - r_j\|_2) \\ \mathbf{x}^i \end{pmatrix} \right\|_2 . \tag{3.9}$$

3.3 Numerical Computations

Using the upper bound obtained from the previous section, we generate a colour map of the numerical values of $E^i(x)$ using the hand example originally shown in the beginning of the chapter. Since the upper bound obtained depends the norm of a vector of the basis functions, it is expected that this norm is the smallest at a point near the centre of mass of the reference landmarks. Figure 3.2 was produced by setting $\epsilon^i = 1$ and $\lambda = 100$.

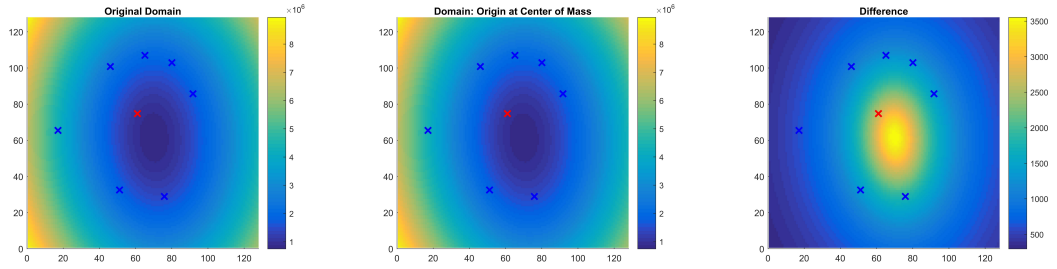

Figure 3.2: Colour map of $E^i(x)$ under the original domain, origin at the centre of mass of landmarks, and their difference.

The left image shows the colour map as-is under the domain $\Omega = [0, 20] \times [0, 25]$ with a 125×125 discretization grid. Then, the domain is translated such that the origin is located at the centre of mass of the reference landmarks. This is shown in the middle image. Finally, the right image shows the difference between the left and middle images. The blue markers denote the location of the reference landmarks, and the red marker is

the location of the centre of mass. A visual inspection of figure 3.2 does confirm that the error bound is minimized near the centre of mass of the landmarks. More precisely, it is minimized where the norm in the error bound attains its global minimum. However, note that the errors in these images are in the order of 10^6. Breaking down the upper bound of equation 3.9, it was discovered that the smallest singular value of L was in the order of 10^{-7}. Hence, dividing by $\sigma_{min}L$ significantly raised the upper bound of $E^i(x)$. This is later confirmed when the condition number of L was computed, which corresponded to $\kappa(L) \approx 2.1 \cdot 10^{11}$. This indicates that there is a huge fluctuation in the eigenvalues of L, thus making eigenvalue/singular value based upper bounds large in numerical value.

Another issue of this upper bound is due to the norm-based approach. Since this approximation is dominated by a norm, the surface generated by the numerical values of the error form a convex surface. This is shown in the images by how numerical values of errors propagate radially outwards from the centre. An ideal result would provide a colour map where the values of the errors are reflected based on the distance from the nearest landmarks. This will emphasize the importance of landmark placements and indicates the confidence of the registration result based on subregions of the image.

Chapter 4

Conclusion and Future Work

4.1 Summary of Results

The use of thin plate splines in image registration provides a transformation that is independent of pixel intensity information. As the name suggests, the regularizer was designed to mimic the bending energy of a thin metal plate. As a result, this registration method is preferred for situations where objects deform nonlinearly in a controlled manner. This was confirmed with the hand example in the previous chapter, where the regularization parameter needed to be manually tuned in order to somewhat maintain the skeletal structure of the hand. For this scenario, an affine-based landmark registration method will yield better results as the transformation will be limited to only sheer, rotation, and translation, which will aid in preserving the rigidness of the bones. On the other hand, TPS excels at registering images of objects where nonlinear deformations are allowed, such as images of brain, muscle, and/or tissue based organs. Depending on the type of tissue present in the images taken, the level of deformation allowed can be controlled simply by adjusting the regularization parameter. Thin plate spline will continue to serve as an extremely valuable registration method as its unique closed form solution provides significantly reduced computation time. This is a huge advantage over

many intensity-based registration techniques which are often ill-posed inverse problems. Due to the iterative nature of these types of problems, it takes much longer to recover feasible functions as candidate solutions.

4.2 Future Work

The original goal of chapter 3 was to find an upper bound of registration errors caused by landmark errors. Using a norm based approach, an upper bound was discovered but concluded that the upper bound was extremely loose. In addition, colour map of the upper bound values did not give clear information on how error-induced landmarks affected the interpolant. Therefore, this cannot be translated to a practical setting. Ultimately, the optimal goal is to determine a much stricter upper bound for the registration error that depends on the distance from the closest landmark. This may allow us to provide a confidence level on accuracy of the registration problem at any location of the image chosen by the user. There are, however, a number of items that will need to be addressed prior to reaching that stage.

- **Numerical values of upper bound**: This will be one of the most important aspects to improve on. Even though the errors were bounded to 1 in a 20×25 domain, the order of the upper bound was in the millions. This was caused primarily due to the poorly conditioned matrix L, where dividing by its smallest singular value dramatically raised the values of the upper bound.

- **Norms of basis functions**: The upper bound obtained in this thesis was essentially a constant multiplied by the norm of the vector of basis functions. It may be beneficial to determine a new upper bound that does not depend on this norm as this leads to error propagating from the point where this vector of basis functions is minimized. As a result, the magnitude revolves around the distance from this central point instead of its distance from the nearest landmark. Weights

that depend on the distance from the landmarks may also be introduced to further improve the error bound. However, these weights must be carefully modelled to preserve mathematical accuracy so they do not appear artificial.

- **Errors in all landmarks**: For the experiments performed, errors were placed only on template landmarks. This was done intentionally as introducing errors to reference landmarks will also change the radial basis functions of the TPS interpolant. The ultimate goal is to provide a general analysis where perturbations are applied to all landmarks, rather than a particular chosen subset.

- **Further study of radial basis kernels and their effects under error**: This will arise naturally by considering errors in all landmarks. Since the radial basis functions are centered around one set of data points, introducing errors to these data points will automatically change the basis functions. In addition, the interpolating matrix will also be affected which may impact its invertibility in the scenario where data points are tightly clustered together.

- **Extension to higher dimensions**: Extension to 3D may prove to be extremely useful clinically. This enables registration of entire 3D objects as opposed to two dimensional slices. Thus allowing accurate registration to fully reconstruct entire organs of interest. In particular, this will greatly aid in tracking internal ailments such as tumours and lesions. It may also be extended to even higher dimensions as this may be valuable in the application of data analytics. Fully understanding how TPS is affected may also assist in generalizing how data errors may affect the class of polyharmonic splines as a whole.

Bibliography

[1] Fred Bookstein. Principal warps: Thin-plate splines and the decomposition of deformations. *IEEE Transactions on Pattern Analysis and Machine Intelligence*, 11(6):567–585, 1989.

[2] Ward Cheney and Will Light. *A Course in Approximation Theory*. 2009.

[3] Jean Duchon. Splines minimizing rotation-invariant semi-norms in sobolev spaces. In *Constructive Theory of Functions of Several Variables*, pages 85–100. Springer, 1977.

[4] Gregory Fasshauer. *Meshfree Approximation Methods with MATLAB*. World Scientific Publishing Company, 2007.

[5] Gregory Fasshauer and Qi Ye. Reproducing kernels of generalized sobolev spaces via a green function approach with distributional operators. *Numerische Mathematik*, 119(3):585–611, 2011.

[6] Jan Modersitzki. *Flexible Algorithms for Image Registration (FAIR)*. Society for Industrial and Applied Mathematics, 2009.

[7] Grace Wahba. *Spline Models for Observational Data*. Society for Industrial and Applied Mathematics, 1990.